remote sensing

MDPI

Article

Early Warning of Anthracnose on *Illicium verum* Through the Synergistic Integration of Environmental and Remote Sensing Time Series Data

Junji Li [1,2], Yuxin Zhao [1], Tianteng Zhang [1], Jiahui Du [1], Yucai Li [1], Ling Wu [1] and Xiangnan Liu [1,*]

[1] School of Artificial Intelligence, China University of Geosciences, Beijing 100083, China
[2] Guangxi Forestry Research Institute, Nanning 530002, China
* Correspondence: liuxn@cugb.edu.cn

Highlights

What are the main findings?

- Proposed an early warning framework for anthracnose on *I. verum* by integrating high-frequency environmental data (meteorological and topographic) with Sentinel-2 time-series imagery.
- Developed an Attention-based Time-Aware LSTM (At-T-LSTM) model that effectively captures temporal dependencies and inter-feature interactions, achieving high accuracy in spatial delineation and temporal early detection.

What are the implications of the main findings?

- The framework enables reliable early detection of anthracnose despite sparse optical observations and weak early-stage spectral responses in cloudy and rainy regions.
- Provides a practical and generalizable tool for precision forestry, supporting the timely risk assessment and sustainable management of *I. verum* and other forest diseases.

Abstract

Anthracnose on *Illicium verum* Hook.f (*I. verum*) significantly affects the yield and quality of *I. verum*, and timely detection methods are urgently needed for early control. However, early warning is difficult due to two major challenges, including the sparse availability of optical remote sensing observations due to frequent cloud and rain interference, and the weak spectral responses caused by infestation during early stages. In this article, a framework for early warning of anthracnose on *I. verum* that combines high-frequency environmental (meteorological and topographical) data and Sentinel-2 remote sensing time-series data, along with a Time-Aware Long Short-Term Memory (T-LSTM) network incorporating an attentional mechanism (At-T-LSTM) was proposed. First, all available environmental and remote sensing data during the study period were analyzed to characterize the early anthracnose outbreaks, and sensitive features were selected as the algorithm input. On this basis, to address the issue of unequal temporal lengths between environmental and remote sensing time series, the At-T-LSTM model incorporates a time-aware mechanism to capture intra-feature temporal dependencies, while a Self-Attention layer is used to quantify inter-feature interaction weights, enabling effective multi-source features time-series fusion. The results show that the proposed framework achieves a spatial accuracy (F1-score) of 0.86 and a temporal accuracy of 83% in early-stage detection, demonstrating high reliability. By integrating remote sensing features with environmental drivers, this approach enables multi-feature collaborative modeling for the risk assessment and monitoring of *I. verum*

check for updates

Academic Editor: Michael Sprintsin

Received: 25 July 2025
Revised: 16 September 2025
Accepted: 18 September 2025
Published: 25 September 2025

Citation: Li, J.; Zhao, Y.; Zhang, T.; Du, J.; Li, Y.; Wu, L.; Liu, X. Early Warning of Anthracnose on *Illicium verum* Through the Synergistic Integration of Environmental and Remote Sensing Time Series Data. *Remote Sens.* **2025**, *17*, 3294. https://doi.org/10.3390/rs17193294

Copyright: © 2025 by the authors. Licensee MDPI, Basel, Switzerland. This article is an open access article distributed under the terms and conditions of the Creative Commons Attribution (CC BY) license (https://creativecommons.org/licenses/by/4.0/).

anthracnose. It effectively mitigates the impact of sparse observations and significantly improves the accuracy of early warnings.

Keywords: Sentinel-2; meteorological data; time-aware long short-term memory (LSTM); attentional mechanism; early warning of forest diseases

1. Introduction

Illicium verum Hook.f (*I. verum*) is an important economic tree species in southern China. In addition to its economic value, *I. verum* also has ecological benefits in terms of soil conservation, soil improvement, climate regulation, and water conservation [1,2]. Guangxi Zhuang Autonomous Region is the largest *I. verum* producing area in China, with the planting area and production accounting for more than 85% of the national total [3,4]. However, the warm and rainy climate in southern China, with high humidity all year round, provides favorable conditions for the growth and spread of pests and diseases. In recent years, the occurrence of anthracnose on *I. verum* has shown an upward trend, resulting in substantial economic and ecological losses [5]. Conventional field-based monitoring methods are limited in spatial and temporal coverage, hindering large-scale, rapid, and accurate anthracnose on *I. verum* detection [6]. Remote sensing technology has emerged as a promising tool for monitoring forest pests and diseases due to its capacity for continuous, large-scale observation [7–9]. When plants are infested, changes in canopy morphology and physiological status induced by stress alter spectral reflectance, enabling the use of vegetation indices and spectral bands to detect infestations [10–14]. Huo et al. proposed Normalized Distance Red and SWIR (NDRS) as a new index based on Sentinel-2 imagery to detect early European spruce bark beetle infestation [15]. Ye et al. used five spectral bands (green, red, NIR, SWIR1, and SWIR2) based on Sentinel-2 imagery as inputs to detect mountain pine beetle disturbance [16]. Li et al. selected the Plant Senescence Reflectance Index (PSRI) and the Fraction of Absorbed Photosynthetically Active Radiation (FAPAR) to detect changes induced by pest and disease stress in *I. verum*, including anthracnose [17]. Extensive research has confirmed that remote sensing could be a valuable and reliable approach for monitoring forest pest and disease outbreaks.

Anthracnose on *I. verum* spreads rapidly, making early identification and intervention essential. A major challenge in remote sensing-based early warning is the limited availability of observational data. To improve temporal resolution, studies often integrate multi-source remote sensing data [18–21]. For example, Ye et al. utilized Landsat-4, -5, -7, and -8 time-series data [16], and Zhao et al. applied a deep learning algorithm to downscale the spatial resolution of Landsat-8 imagery to 10 m, and subsequently interpolated it with Sentinel-2 imagery to achieve higher temporal resolution for monitoring forest pests [21]. However, the approach of synergistic multi-source remote sensing data has inherent shortcomings. Firstly, due to the differences in different sensors and the errors caused by interpolation algorithms, the interpolated data have certain errors, and the weak spectral changes caused by early-stage infestation may further deepen the misdetection and omission. Moreover, for the situation of cloudy and rainy conditions (e.g., in the southern region of China), even if synergized, multi-source optical remote sensing data cannot satisfy the demand of high-frequency observation in the early stage of disease [22].

Meteorological factors, including temperature and precipitation, have been proved to be important predisposing factors for anthracnose on *I. verum* [23,24]. In more detail, under the conditions of temperature above 15 °C and humidity above 70%, the pathogenic spores begin to germinate and spread. Under the warm, hot, and humid climatic conditions in

late spring, the germination and spread of the pathogenic spores accelerate, and *I. verum* trees are thus susceptible to anthrax infection [24]. In addition, topographical factors, including DEM, aspect, and slope also have an impact on the occurrence of anthracnose on *I. verum* [25]. In areas with limited sunlight, *I. verum* tends to grow weakly and is more susceptible to disease infection. In contrast, at higher elevations, with lower temperatures, the germination and spread of pathogenic spores are restricted, resulting in a relatively lower incidence of anthracnose. However, most of the existing studies utilizing environmental data (meteorological and topographical) have focused on the evaluation of pests and the disease risk or prediction of regional incidence [24,26–32]. For example, Meynard et al. predicted the potential geographic distribution of desert locusts based on meteorological factors by using a variety of niche models [27]; Shen et al. assessed the risk area of pine wood nematode by integrating meteorological, topographic, and human activities and other sources of geographic information [28]. There is a lack of research on early warning or monitoring of pests and diseases based on environmental data. Compared with remote sensing data, which could accurately detect the changes occurring, environmental data monitors the ground surface at a daily time resolution, which could give timely warnings of the changes occurring. Thereby, some scholars have combined climate data and remote sensing data to carry out pest and disease monitoring studies [29–32], including Shen et al., who synergized multi-source remote sensing data, meteorological data, and soil data for the modeling of a habitat suitability evaluation of pests and diseases on a regional scale [22]. Therefore, the integration of high-temporal-resolution meteorological data, which are closely associated with the onset of anthracnose on *I. verum*, and remote sensing time-series data, which are sensitive to the disease response, is expected to provide dense observational information, thereby enabling early warning of pest and disease outbreaks at accurate locations.

In terms of existing pest detection, algorithms mostly rely on time-series change detection techniques, including COLD (Continuous Land Disturbance Detection) [33], SCCD (Stochastic Continuous Change Detection) [16], EWMACD (Exponentially Weighted Moving Average Change Detection) [34], etc. These methods detect anomalous changes by analyzing historical observations of the target location and constructing a change baseline. Although these methods have achieved some success in specific scenarios, they have a high dependence on the quantity and quality of historical data. For example, the COLD algorithm requires at least 15 views of valid observation images to achieve the model initialization, which is difficult to satisfy in cloudy and rainy areas. At the same time, although the algorithm supports multi-feature inputs, it requires that all the features are time-aligned, which has a high quality dependence on the data [16]. Environmental and remote sensing data have different temporal resolutions, forming a non-equally spaced multi-source time series. For example, meteorological data are on a daily scale, while remote sensing images such as Sentinel-2 are on a five-day view under ideal conditions, and with irregular intervals in reality. This temporal resolution inconsistency poses a great challenge to time-series change detection algorithms in terms of feature alignment and joint modeling. In recent years, deep learning algorithms have been widely used in the field of change detection due to their automatic feature extraction, nonlinear modeling capability, and strong generative ability [35]. Aiming at the problem of uneven feature time intervals, the T-LSTM (Time-Aware Long Short-Term Memory) network has been proposed, which improves the structure of the traditional LSTM and introduces a time-aware module so that it can effectively model single feature sequences with non-equally spaced time steps [36]. The different temporal resolution between remote sensing and environmental data causes the number of features to vary significantly from time step to time step, so it is difficult for a single time-aware mechanism to comprehensively capture the asynchronous dynamic

associations between various types of features. The Attention mechanism provides the model with the ability to weight the feature dimension outside the time dimension for modeling, and can dynamically learn the importance of features at different time points and from different sources, thus achieving effective synergy between multiple features [37]. Based on this, combining the T-LSTM network with the Attention mechanism not only adapts to the non-equal-interval characteristics of remote sensing and environmental data in the time dimension, but also flexibly selects the most representative subset of features at different time steps, thus improving the ability of multi-source irregular time-series modeling in early warning of forest diseases.

Aiming to address the problem of sparse optical remote sensing observations in cloudy and rainy regions, which affects the early warning of anthracnose on *I. verum*, this study analyzes the early-stage characteristics of the disease and identifies meteorological factors that induce its occurrence and have high observation frequency as sensitive features. The At-T-LSTM model, which combines the T-LSTM network with the Attention mechanism, is introduced to achieve multi-feature synergy for risk assessment and early warning of anthracnose on *I. verum*. By integrating habitat-related information such as meteorological variables and remote sensing features, this approach aims to enhance early warning accuracy through synergistic multi-feature monitoring and the development of an early warning technology for anthracnose on *I. verum*.

2. Study Area and Data

2.1. Study Area

The study area is located within the Liuwandashan National Forest Park, Guangxi Zhuang Autonomous Region, China (Figure 1). It covers a total area of approximately 29 km^2, including about 8.28 km^2 of *I. verum* plantations. The region falls within the southern subtropical monsoon climate zone, with an average annual temperature of 21.5 °C and annual precipitation ranging from 1600 to 1800 mm. More than 75% of the annual rainfall occurs between April and September. Elevation in the study area ranges from 200 to 850 m, and the terrain is dominated by low mountains and hilly landscapes, with slopes mostly between 15° and 35°. Anthracnose on *I. verum* occurs frequently in the study area [17], exhibiting distinct seasonal patterns. Initial symptoms typically appear in mid-March and become more pronounced by early May. This period also marks the first recommended window for fungicide application, making it a critical stage for disease prevention and control.

2.2. Sentinel-2 Data

Based on long-term observations from the forest farm, the early stage of anthracnose on *I. verum* typically occurs from mid-March to the end of June. Accordingly, Sentinel-2 L2A imagery from mid-March to the end of June in 2018 and 2019 was selected to match the physiological cycle of the disease. The temporal distribution of the images is shown in Table 1. Imagery with cloud cover less than 40% over the study area was acquired through the Google Earth Engine (GEE) platform and processed using the Fmask algorithm for cloud removal. Only 23 usable scenes were obtained during the critical disease window over the two-year period, averaging 2.3 valid scenes per month—significantly lower than the theoretical revisit frequency of Sentinel-2. Notably, observation gaps exceeded 10 days during key outbreak periods, and the overall time series exhibited an uneven temporal distribution.

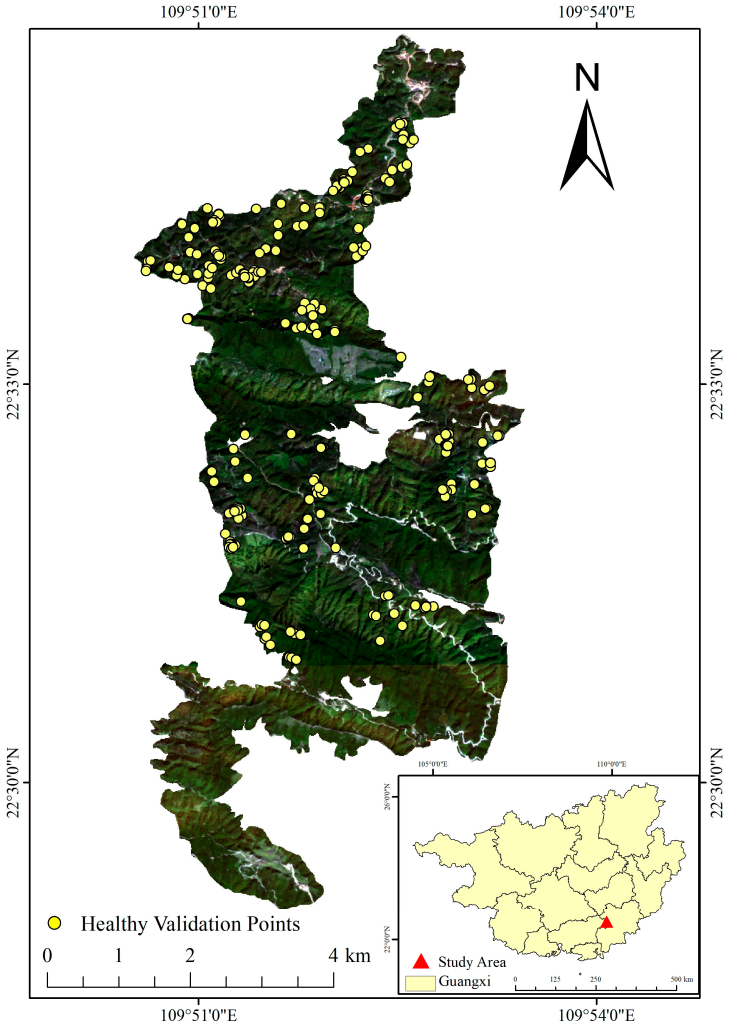

Figure 1. Geographic location of the study area and distribution of the validation samples for anthracnose on *I. verum*. Yellow points represent the validation sample. The background image is a Sentinel-2 image acquired in 2019 (RGB = band red, green, and blue).

Table 1. Monthly distribution of available Sentinel-2 imagery dates.

Year	**2018**				**2019**			
Month	March	April	May	June	Marth	April	May	June
Number of Images	1	4	3	3	1	4	3	4

2.3. Environmental Data

Environmental data includes both meteorological and topographic data. The meteorological data were obtained from a high-resolution (1 day, 1 km) and long-term (1961–2019) dataset gridded for temperature and precipitation across China (HRLT) [38], which provides values of maximum temperature, minimum temperature, and precipitation. The meteorological data were resampled to a spatial resolution of 10 m using the nearest neighbor method. Topographic data were obtained from the Shuttle Radar Topography Mission (SRTM) Digital Elevation Model (DEM). It was acquired through the GEE platform. Slope and aspect were calculated based on the DEM. The original spatial resolution of the data was 30 m, and it was resampled to a spatial resolution of 10 m using the nearest neighbor method.

2.4. Training, Validation Data and Forest Mask

With the assistance of forest farm staff, field surveys on anthracnose on *I. verum* were conducted in the study area from March to July in both 2018 and 2019. The coordinates of sample plots and the occurrence of disease and pest symptoms were recorded using the Ovitalmap (V10.3.6) mobile application. A total of 300 early-stage disease sample points and 300 healthy points were collected. The dataset was then divided into a training set and a validation set at a ratio of 8:2.

Since the focus of this study is on the early warning of anthracnose on *I. verum*, and the forested areas in the study area are dominated by pure *I. verum* stands, an *I. verum* forest mask was generated by intersecting forest cover layers extracted from the ESRI land use/land cover (LULC) dataset during 2018 and 2019 (10 m resolution). This intersection was further refined using manually interpreted corrections based on field-surveyed *I. verum* sample points.

3. Methodology

The overall workflow of this study is illustrated in Figure 2. First, a variety of vegetation indices sensitive to forest disease were calculated from Sentinel-2 time-series imagery. Then, combined with meteorological and topographic data, a set of features with high sensitivity to early-stage anthracnose on *I. verum* was selected to construct a sensitive feature time series for disease monitoring. Next, to address challenges such as non-uniform time intervals and inconsistent numbers of features at different time steps in the remote sensing and meteorological data, the T-LSTM network, which was adapted for irregular time series, was enhanced with an Attention mechanism to develop the At-T-LSTM model (the detailed mechanisms of the model are elaborated in Section 3.3.2). The Attention mechanism dynamically assigns weights to environmental and remote sensing features, enabling early warning of anthracnose on *I. verum*. The following sections will delve into the key processes in detail.

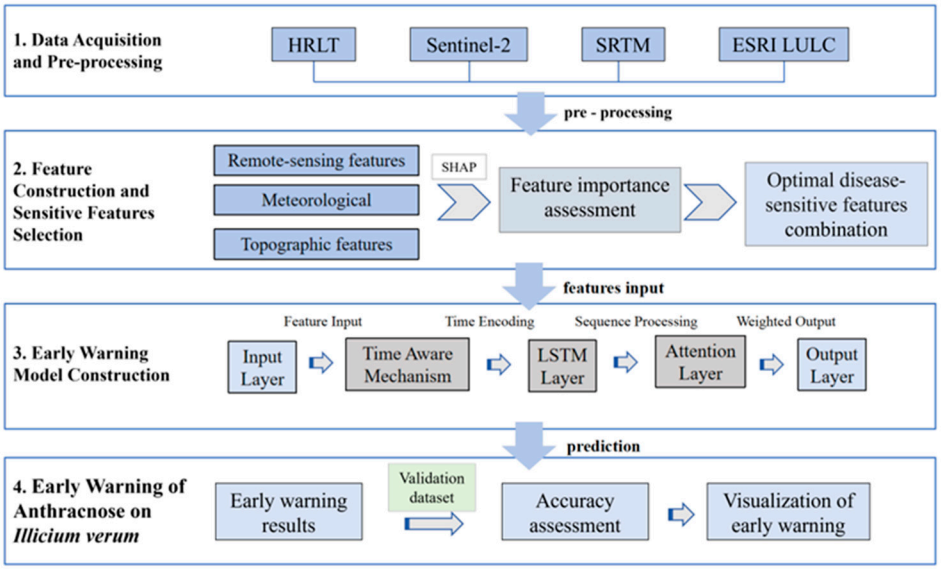

Figure 2. Flowchart for early warning of anthracnose on *I. verum* based on the At-T-LSTM model. The workflow integrates Shapley Additive Explanations (SHAP) to assess feature contributions, which are further described in Section 3.2.

3.1. Calculation of Vegetation Indices Sensitive to Anthracnose on I. verum

Anthracnose on *I. verum* induces a series of physiological, biochemical, and morphological changes, leading to changes in spectral reflectance, which provides a crucial basis

for remote sensing to detect early infection. Specifically, in the early stages of infection, *I. verum* activates defense mechanisms that trigger chlorophyll degradation, carotenoid imbalance, and a decrease in cellular water content. These physiological responses are often accompanied by metabolic dysfunctions such as impaired photophosphorylation, abnormal stomatal conductance, and unbalanced transpiration rates [39,40], which lead to changes in vegetation indices. In terms of morphology, small irregular dark brown lesions begin to show on the green leaves, and the spectral signature exhibits a shift in the "green peak" toward the red band. The spectral differences between healthy and anthracnose-infected *I. verum* plants are illustrated in Figure 3.

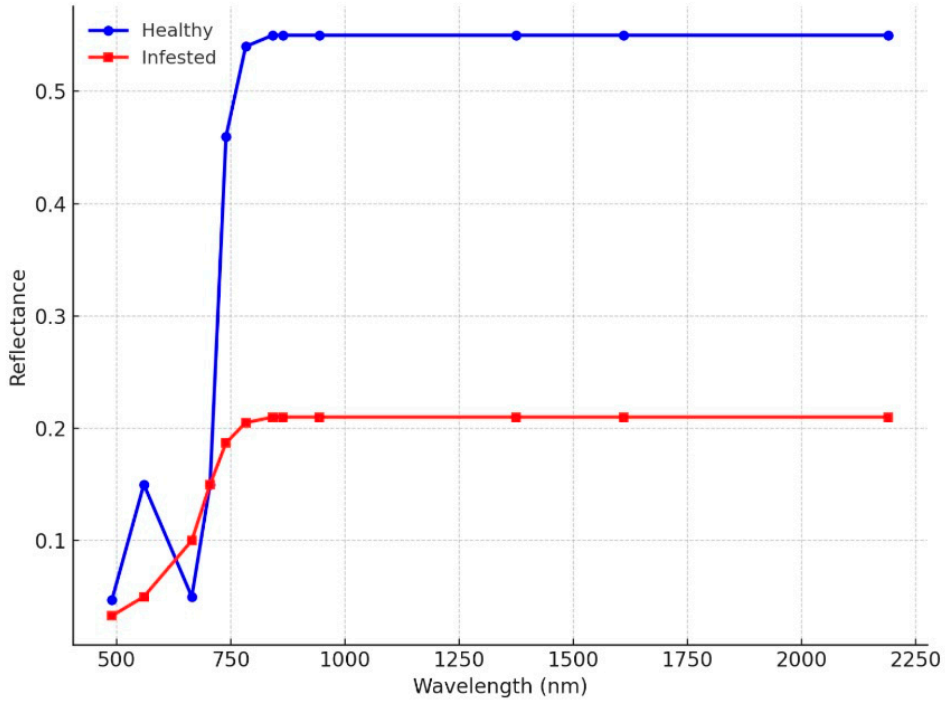

Figure 3. Spectral reflectance differences between healthy and anthracnose-infected *I. verum* based on Sentinel-2 data.

To improve the responsiveness to the symptoms of early-stage anthracnose on *I. verum*, and with reference to previous studies [41–44], three vegetation indices, including the Enhanced Vegetation Index (EVI), Normalized Burning Ratio (NBR), and Red-Green Ratio Index (RGI), were selected for calculation and analysis. The specific formulas are shown in Table 2.

Table 2. The candidate features for detecting anthracnose infestation.

Index	Formulation	Indicated Change	Relevance to Anthracnose Detection
EVI	$\frac{2.5(\mathrm{NIR}-\mathrm{Red})}{(\mathrm{NIR}+6\ \mathrm{Red}-7.5\ \mathrm{Blue})-1}$	Blade structure	Detects microstructural changes in canopy caused by hyphal penetration and cell destruction during early infection
RGI	$\frac{\mathrm{Red}}{\mathrm{Green}}$	Coloration	Sensitive to chlorosis and dark lesion formation characteristic of anthracnose
NBR	$\frac{\mathrm{NIR}-\mathrm{SWIR2}}{\mathrm{NIR}+\mathrm{SWIR2}}$	Moisture stress and blade structure	Captures water regulation disruption and necrosis caused by infection

3.2. Selection of Optimal Sensitive Feature Combination

To improve the response capability and discrimination accuracy of the early warning model for anthracnose on *I. verum*, candidate features from remote sensing, meteorological, and topographic data were selected. Remote sensing features include the EVI, NBR, and RGI, which reflect the physiological state of vegetation and spectral variations associated with disease stress. Meteorological features, including maximum temperature, minimum temperature, and precipitation, describe environmental conditions favorable for disease development. Topographic features, including DEM, slope, and aspect, are used to capture the influence of terrain on local microclimate and soil moisture distribution, which indirectly affect disease occurrence and progression.

Shapley Additive Explanations (SHAP) is a method for interpreting the output of machine learning models. Based on the Shapley value theory from cooperative game theory, SHAP quantifies the contribution of each input feature to model predictions by calculating its marginal effect. This approach provides a scientifically grounded basis for feature selection and supports the construction of an optimal feature subset for model performance improvement [45–47].

During the feature selection process, the machine learning model is interpreted using the SHAP method applied to the initial model trained on the dataset. By evaluating the contribution of each feature index, the top-ranking features are retained to form a set with the highest discriminative power for the early detection of anthracnose on *I. verum*. The SHAP formula is as follows:

$$\phi_j = \sum_{S \subseteq N \setminus \{j\}} \frac{|S|(n-|S|-1)!}{n!} [f(S \cup \{j\}) - f(S)] \quad (1)$$

where S represents any subset of all features excluding feature j; $|S|$ denotes the number of features in subset S; N is the full set of input features; $f(S)$ indicates the prediction output of the machine learning model when only features in subset S are used; and $f(S \cup \{j\}) - f(S)$ reflects the marginal contribution of feature j to the model's prediction when added to subset S.

3.3. Attention-Based Time-Aware Long Short-Term Memory (At-T-LSTM) Model

In this paper, remote sensing and environmental data are synergized to achieve early warning of anthracnose infestation on *I. verum*, where remote sensing and environmental data are non-equally spaced time distributions. The T-LSTM model is used to deal with multi-source time series composed of remotely sensed vegetation indices, meteorological variables, and terrain data. Furthermore, in order to achieve dynamic synergy among multiple features, the model introduces an Attention mechanism that fuses the contributions of each feature to anthracnose risk early warning and monitoring at different times, providing support for early warning in high-frequency and complex disturbance contexts.

3.3.1. Time-Aware Long Short-Term Memory (T-LSTM) Model

The structure of the T-LSTM model is shown in Figure 4. Assuming that at the disease detection time step t, the input features (including vegetation index, temperature, humidity, etc.) at the current moment are x_t, the hidden state of the previous time step is h_{t-1}, the state of the memory cell is C_{t-1}, and the time interval is Δt at the satellite revisit period or the environmental data observation interval, the computational procedure of T-LSTM is as follows.

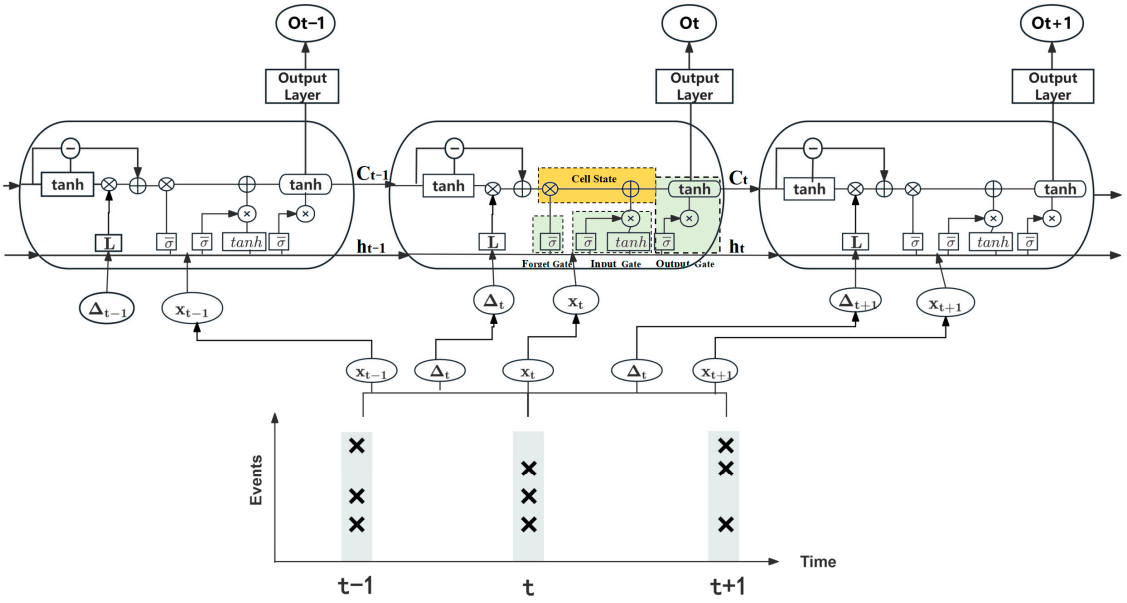

Figure 4. Structure of the T-LSTM network.

First, the time-aware factor d_t is computed as follows:

$$d_t = \exp(-W_d \Delta t + b_d) \tag{2}$$

where W_d is the time-aware weight matrix and b_d is the bias term. The time-aware coefficient d_t is a value between 0 and 1 that models the natural awareness of environmental states over time. This coefficient is used to dynamically adjust the memory cell state:

$$c_{t-1}^{decay} = d_t \odot c_{t-1} \tag{3}$$

where $\odot$ denotes element-wise multiplication. The time-aware memory cell state c_{t-1}^{decay} quantifies the influence of the time interval Δt on the memory of historical environmental states. Through this step, the T-LSTM dynamically adjusts the memory cell state. When the time intervals are longer, the awareness of historical information is stronger, conversely, the awareness is weaker, thus effectively capturing the dependent changes caused by uneven time distribution in remote sensing data.

Subsequently, the T-LSTM computes the forget gate f_t, input gate i_t, candidate memory state $\widetilde{c}_t$, and output gate o_t in a manner similar to the standard LSTM. The general form is as follows:

$$g_t = \phi\left(W_g \cdot [h_{t-1}, x_t] + b_g\right) \tag{4}$$

where $g_t \in \left\{f_t,\ i_t, \widetilde{c}_t, o_t\right\}$, W_g and b_g are the corresponding weight matrix and bias term, and ϕ is the activation function. Specifically,

For the forget gate f_t, $\phi = \sigma$, controlling the retention of decayed historical state information.

For the forget gate i_t, $\phi = \sigma$, regulating how much new environmental information enters the memory.

For the forget gate $\widetilde{c}_t$, ϕ = tanh, computing the latent environmental update.

For the forget gate o_t, $\phi = \sigma$, determining how much information is passed to the hidden state.

To update the memory cell state c_t and the hidden state h_t:

$$c_t = f_t \odot c_{t-1}^{decay} + i_t \odot \widetilde{c}_t \tag{5}$$

$$h_t = o_t \odot \tan h(c_t) \tag{6}$$

The updated memory state c_t combines the past disease risk trends with the latent anomalies observed at the current time step, while the hidden state h_t represents the output of the T-LSTM at the current time step.

3.3.2. Incorporating Attention Mechanism into T-LSTM Model

The integration of an Attention mechanism was motivated by three fundamental limitations inherent in conventional change detection methods when applied to multi-source forest disease monitoring. First, the significant temporal misalignment between high-frequency environmental data (e.g., daily meteorological measurements) and irregular remote sensing observations creates spatiotemporal gaps that conventional methods cannot adequately address. Second, the varying informational relevance of different features at distinct phenological stages requires dynamic feature weighting capabilities beyond static parametric approaches. Third, the weak spectral signals characteristic of early disease infestation are often obscured within complex environmental backgrounds, demanding enhanced feature discrimination capabilities.

The Attention mechanism addresses these limitations through two principal innovations: (1) It enables learnable temporal alignment of heterogeneous data streams through context-aware feature weighting, effectively mitigating the temporal resolution disparities that constrain conventional methods. (2) It provides explicit quantification of feature significance across temporal contexts, allowing the model to dynamically prioritize the most informative biomarkers and environmental drivers during different phenological stages, which is particularly crucial for detecting subtle physiological changes preceding visible symptom development.

On the basis of modeling each single feature separately by using the T-LSTM network to capture its time-series evolution law, we introduce an Attention mechanism (Figure 5), which dynamically assigns feature weights to enable the model to learn the importance of the features from different sources at different points in time.

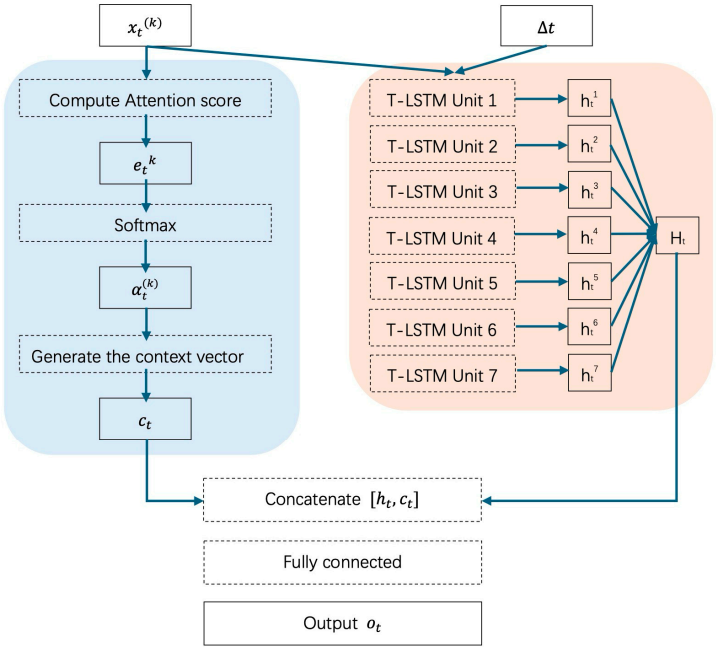

Figure 5. The structure of the Attention-based Time-Aware Long Short-Term Memory Model.

The core idea of the Attention mechanism is to dynamically assign weights by computing the relevance between the hidden states at each time step and the current task. Specifically, the Attention mechanism operates as follows:

At each time step, an Attention score $e_t^{(k)}$ is computed for each remote sensing and environmental feature $x_t^{(k)}$, reflecting its importance in the assessment of anthracnose disease risk and symptom monitoring. These Attention scores are then normalized using a Softmax function to obtain the corresponding Attention weights $\alpha_t^{(k)}$. Based on these weights, a weighted sum of the feature representations $x_t^{(k)}$ is calculated to generate the context vector c_t.

$$c_t = \sum_{k=1}^{K} \alpha_t^{(k)} x_t^{(k)} \tag{7}$$

The fused context vector c_t integrates the most informative signals from the multi-source features at the current time step. It is then concatenated with the hidden state h_t output by the T-LSTM to form the final representation, which is used for predicting the risk of anthracnose on *I. verum*.

$$o_t = W_o \cdot [h_t, c_t] + b_o \tag{8}$$

where W_o represents the weight matrix and b_o represents the bias term.

Through this mechanism, the model can adaptively focus on the contributions of different features across time, thereby improving the accuracy and sensitivity of temporal disease recognition. This approach is well-suited for early warning scenarios characterized by uneven temporal feature distributions and complex response mechanisms.

The proposed At-T-LSTM model was implemented with the following hyperparameters: two stacked LSTM layers with 256 hidden units each, utilizing Softmax activation. The model was optimized using AdamW with a learning rate of 1×10^{-5}. Training was conducted for a maximum of 150 epochs with a batch size of 32, employing an early stopping callback (patience = 15) monitored on validation loss to prevent overfitting. This configuration was determined to be optimal through validation set evaluation.

3.4. Accuracy Assessment and Analysis

3.4.1. Accuracy Assessment

To assess the spatial accuracy of early warning results, the Precision, Recall, and F1-score were computed as accuracy evaluation metrics based on the validation dataset. Precision measures the proportion of predicted infected areas that are actually infected, while Recall measures the proportion of truly infected areas that are correctly identified. The F1-score is the harmonic mean of Precision and Recall, providing a balanced metric that is especially informative for situations where class distribution is imbalanced or both false positives and false negatives are critical to avoid.

$$Precision = \frac{TP}{TP + FP} \tag{9}$$

$$Recall = \frac{TP}{TP + FN} \tag{10}$$

$$F1 - score = \frac{2 \times TP}{2 \times TP + FP + FN} \tag{11}$$

where TP represents true positive, FP represents false positive, and FN represents false negative.

3.4.2. Multidimensional Method Comparison

To validate the effectiveness of the proposed data synergy strategy, this study implements a dual-level comparative framework. First, we compare the spatial and temporal accuracy achieved using only Sentinel-2 data versus the combined use of Sentinel-2 and environmental data within the At-T-LSTM model, thereby isolating and quantifying the specific contribution of multi-source data integration.

Building upon this foundation, the present study compares the proposed method with two representative approaches widely applied in remote sensing time-series change detection—COLD and EWMACD. These methods have demonstrated particular effectiveness in forest disturbance monitoring and pest detection tasks, making them highly relevant benchmarks for our specific application context. Also, as traditional threshold-based methods relying exclusively on remote sensing data, they provide a fundamental technical contrast to our proposed deep learning approach that integrates multi-source data, thereby enabling a clearer evaluation of the innovation and advantages of our method. Due to the input constraints of the COLD and EWMACD algorithms, which are designed for single-source remote sensing data analysis, this comparison exclusively employs Sentinel-2 data as model input for all methods to ensure a fair and controlled performance evaluation.

To verify whether the improvements of AT-T-LSTM over traditional change-detection methods (COLD and EWMACD) at the pixel level are statistically significant, we employed the McNemar paired chi-square test. For the two comparisons (AT-T-LSTM vs. COLD and AT-T-LSTM vs. EWMACD), 2×2 contingency tables were constructed by counting the number of validation samples correctly/incorrectly classified by method A but incorrectly/correctly classified by method B. Since the sum of discordant pairs (b + c) exceeded 25 in all comparisons, satisfying the large-sample approximation condition, the chi-square statistic was directly used for two-tailed tests with a significance level of $\alpha = 0.05$.

4. Results

4.1. Feature Selection Results

Figure 6 displays the feature contribution ranking in early-stage disease identification of *I. verum*, derived from an LSTM model integrated with SHAP algorithm for interpretability analysis. This enables quantitative identification of key variables exerting significant influence on model predictions.

As evidenced in the figure, the Enhanced Vegetation Index (EVI) exhibits the highest SHAP value contribution among all features, indicating its critical role in early-stage disease identification of *I. verum*. This is consistent with the known physiological responses of infected plants, where chlorophyll degradation, impaired photosynthesis, and reduced canopy greenness occur at early stages, all of which are directly captured by the EVI. The Normalized Burn Ratio (NBR) ranks second, reflecting its sensitivity to tissue necrosis and water loss that alter near-infrared and shortwave-infrared reflectance during early pathogenesis. Daily maximum temperature and precipitation rank third and fourth with SHAP values. Their importance aligns with the established epidemiology of *I. verum* anthracnose: warm and humid conditions accelerate spore germination, dispersal, and host infection. In contrast, topographic factors show lower contributions due to their temporal invariance, though they may influence background susceptibility by modifying microclimate. The dominance of the EVI, NBR, maximum temperature, and precipitation demonstrates that the most informative predictors of anthracnose onset are those directly linked to host physiological stress and pathogen-conducive environments, providing a mechanistic basis for the feature selection results.

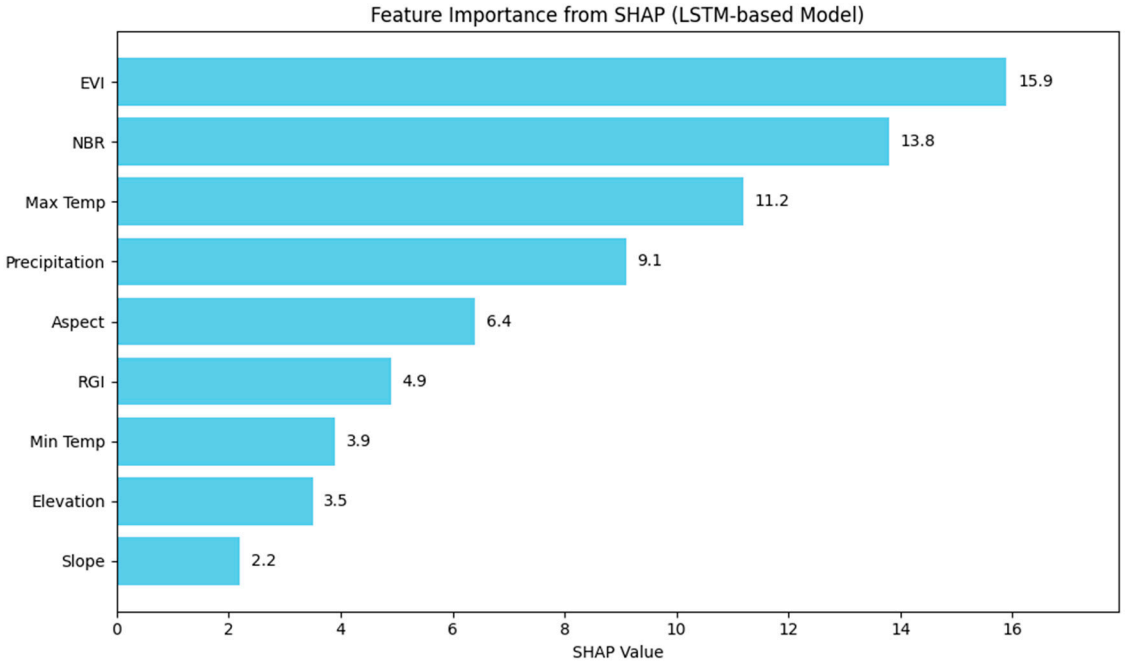

Figure 6. Contribution of each feature based on SHAP algorithm.

4.2. Spatial Accuracy Assessment of Anthracnose on I. verum Detection

4.2.1. Spatial Accuracy Assessment

Table 3 presents the spatial accuracy assessment results of the At-T-LSTM algorithm. For anthracnose-infected *I. verum* sample points, the producer's accuracy (PA) and user's accuracy (UA) reached 0.85 and 0.87, respectively, while healthy samples attained PA = 0.86 and UA = 0.85. With an F1-score of 0.86, the At-T-LSTM algorithm demonstrates effective capabilities for agroforestry pest monitoring.

Table 3. Spatial accuracy assessment results.

Label \ Test Result	Infested Point	Healthy Point	Total	User's Accuracy
Infested point	52	8	60	0.87
Healthy point	9	51	60	0.85
Total	61	59		
Producer's accuracy	0.85	0.86	F1-score	0.86

4.2.2. Comparison of Spatial Accuracy Between Multi-Source Synergistic Data and Standalone Remote Sensing Data

In order to investigate whether the addition of environmental data improves the spatial accuracy of early warning, the study compared the performance of the model combining environmental and remote sensing data with that using remote sensing data alone for early anthracnose detection (Table 4). Compared to the model using only remote sensing data, the synergistic strategy significantly reduced omission and commission errors, indicating that relying solely on remote sensing data suffers from insufficient recognition capability. The integration of environmental factors with remote sensing data enhanced the model's sensitivity and recognition ability for subtle disease signals.

Table 4. Comparison of spatial accuracy between synergistic data and standalone remote sensing data. Env–Remote Sensing: environment and remote sensing data. A total of 120 validation sample points (60 diseased and 60 healthy) were used.

	Env–Remote Sensing	Remote Sensing
Precision	0.85	0.73
Recall	0.87	0.77
OA	0.85	0.74
F1-Score	0.86	0.75

Figure 7 demonstrates typical cases of the At-T-LSTM algorithm in detecting anthracnose on *I. verum* using single remote sensing data sources versus collaborative environment and remote sensing data. The detection results based on collaborative data significantly reduce omission errors and exhibit increased clustering with contiguous distribution, aligning with the epidemic pattern of *I. verum* anthracnose. This indicates that integrating environmental factors enhances the diversity of disease features.

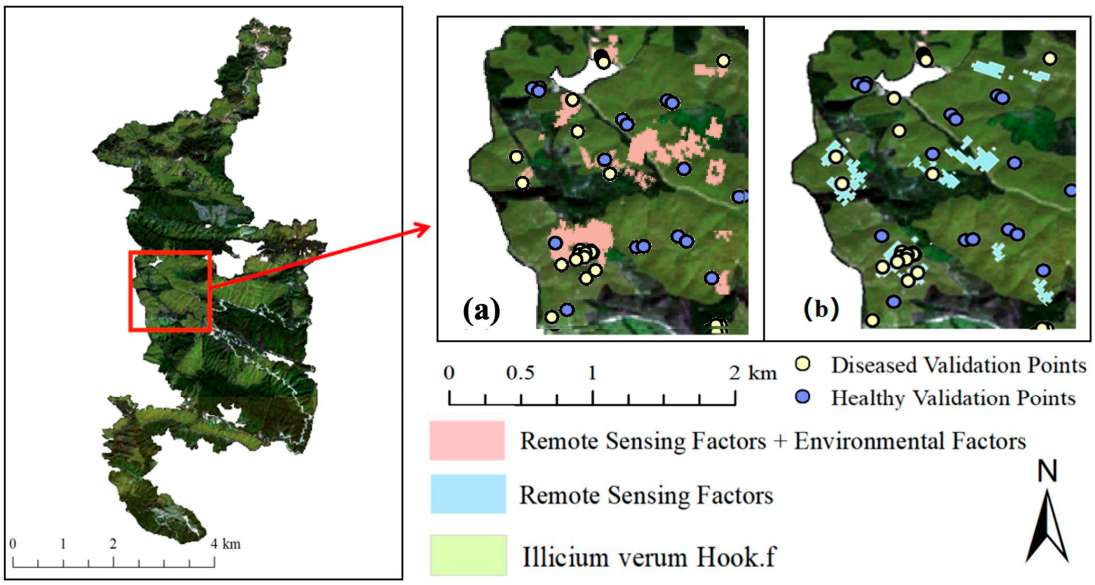

Figure 7. Spatial accuracy comparison in a typical anthracnose-infected area of *I. verum*: (**a**) integrated environment-remote sensing data and (**b**) single remote sensing model for early warning.

4.2.3. Comparison of Spatial Accuracy Between At-T-LSTM and Time Series Change Detection Algorithms

To validate the advancement of the proposed algorithm, this study compared its spatial accuracy in detecting early-stage anthracnose on *I. verum* with two state-of-the-art time-series change detection methods, COLD and EWMACD, which are currently the most effective for early pest monitoring. As illustrated in Figure 8, the proposed At-T-LSTM algorithm achieved the highest performance and significantly outperformed the time-series change detection algorithms. This demonstrates the effectiveness of the Attention mechanism and time decay mechanism, confirming At-T-LSTM as a highly applicable method for early-stage disease detection.

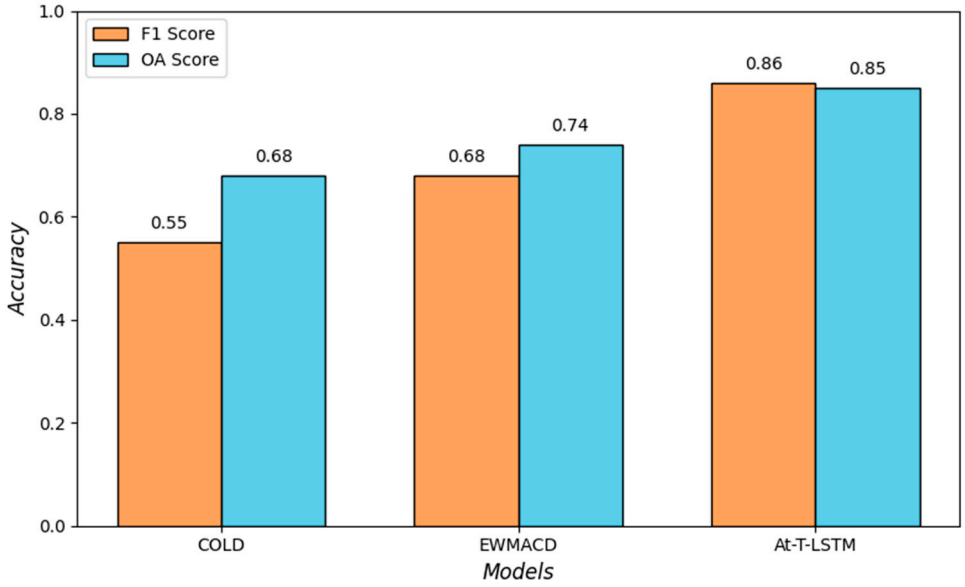

Figure 8. Performance comparison results between At-T-LSTM with COLD and EWMACD algorithms.

We selected a typical disease area to demonstrate the spatial accuracy comparison results, as shown in Figure 9. For early-stage anthracnose detection, both EWMACD and COLD algorithms exhibited severe omission errors and highly fragmented distributions, likely due to their insensitivity to subtle changes caused by early disease symptoms. In contrast, the At-T-LSTM algorithm achieved the lowest omission error rate and demonstrated superior overall accuracy.

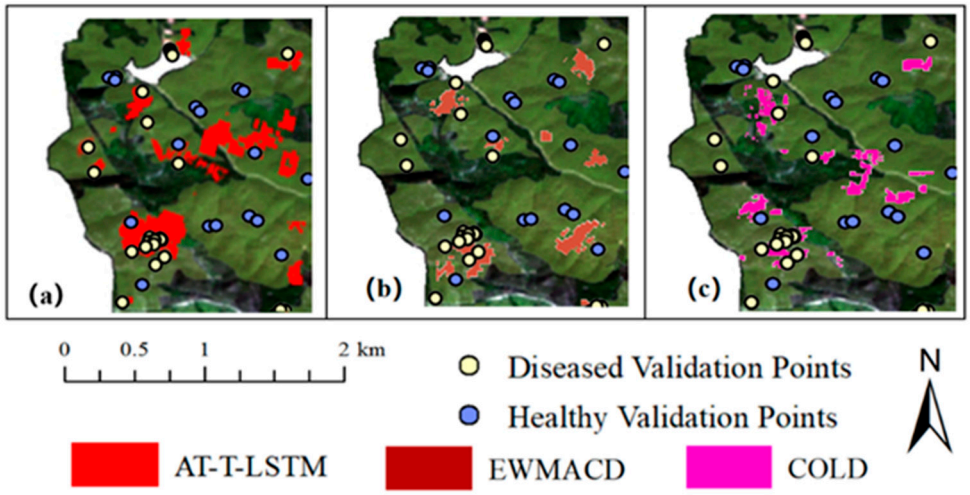

Figure 9. Spatial accuracy comparison of At-T-LSTM versus COLD and EWMACD in early warning of infestation. Detection results based on (**a**) At-T-LSTM, (**b**) EWMACD, and (**c**) COLD algorithm.

McNemar's test was conducted to statistically compare per-sample classification outcomes among the three methods, with a significance threshold of $\alpha = 0.05$. The result is shown in Table 5. For AT-T-LSTM vs. COLD, the test yielded $\chi^2 = 3.77$, $p = 0.052$, indicating a near-significant improvement of AT-T-LSTM. For AT-T-LSTM vs. EWMACD, the test yielded $\chi^2 = 4.67$, $p = 0.031$, confirming that AT-T-LSTM significantly outperformed EWMACD. Finally, the comparison between COLD and EWMACD yielded $\chi^2 = 5.76$, $p = 0.016$, suggesting that EWMACD is also significantly better than COLD.

Table 5. McNemar's test results on the validation set (α = 0.05).

Comparison	b (A Correct, B Wrong)	c (A Wrong, B Correct)	b + c	χ^2	*p*-Value
AT-T-LSTM vs. COLD	33	19	52	3.77	0.052
AT-T-LSTM vs. EWMACD	28	14	42	4.67	0.031
COLD vs. EWMACD	24	10	34	5.76	0.016

4.3. Temporal Accuracy Assessment of Anthracnose on I. verum Detection

4.3.1. Temporal Accuracy Assessment

Temporal accuracy evaluation of the algorithm was conducted, with results detailed in Table 6. For the spatial accuracy assessment, 52 validation points were accurately monitored to statistically analyze the algorithm's detection performance across different time windows. The results demonstrate that 43 points (83%) were successfully detected during the early symptomatic phase of anthracnose, indicating high responsiveness of our algorithm to initial disease onset.

Table 6. Temporal accuracy assessment results of At-T-LSTM. Env–Remote Sensing: environment and remote sensing data.

	Early Stage		Mid to Late Stage		Total	
	Remote Sensing	Env–Remote Sensing	Remote Sensing	Env–Remote Sensing	Remote Sensing	Env–Remote Sensing
Detected Point	32	43	14	9	46	52
Proportion	70%	83%	30%	17%	100%	100%

4.3.2. Comparison of Temporal Accuracy Between Multi-Source Synergistic Data and Standalone Remote Sensing Data

Table 6 presents the temporal accuracy evaluation results of the At-T-LSTM model, comparing the detection performance across disease progression stages under two input strategies: synergistic remote sensing and environment data versus remote sensing data alone. The analysis is based on 52 validation points successfully detected through environmental-remote sensing synergy in spatial accuracy assessment and 46 points detected using only remote sensing. Results demonstrate that during the early symptomatic phase, the data synergy strategy increases temporal accuracy by 13%. This enhancement confirms that integrating multi-source temporal information effectively captures early-stage infestation signals, significantly improving the model's early-warning capability for preemptive disease control.

4.3.3. Comparison of Temporal Accuracy Between At-T-LSTM Model and Time-Series Change Detection Algorithms

The study selected a disease point consistently detected by At-T-LSTM, COLD, and EWMACD algorithms. As shown in Figure 10, the At-T-LSTM model still demonstrated the highest temporal accuracy, with its predicted or early-warning time points occurring significantly earlier than those identified by the two time-series change detection methods. This indicates that the At-T-LSTM model holds an advantage in extracting predictive early-stage temporal features, enabling earlier identification of impending change signals.

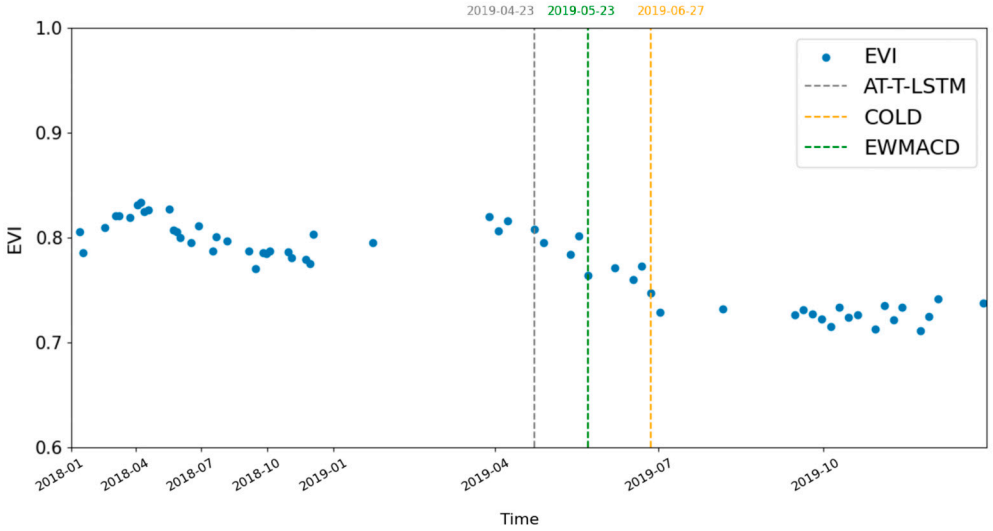

Figure 10. The onset response timing of At-T-LSTM, EWMACD, and COLD algorithms at typical disease points.

The study demonstrates the temporal accuracy comparison of different models by presenting disease detection results at two distinct time points in a typical disease-affected area. As shown in Figure 11, At-T-LSTM detected a sufficient number of early-stage disease symptoms by May 13, while the EWMACD and COLD algorithms identified only limited disease manifestations on the same date. Through comparative analysis between ground-truth disease points and classification results, At-T-LSTM detected early disease symptoms approximately 25 days earlier than the other models, confirming its superior temporal accuracy over EWMACD and COLD.

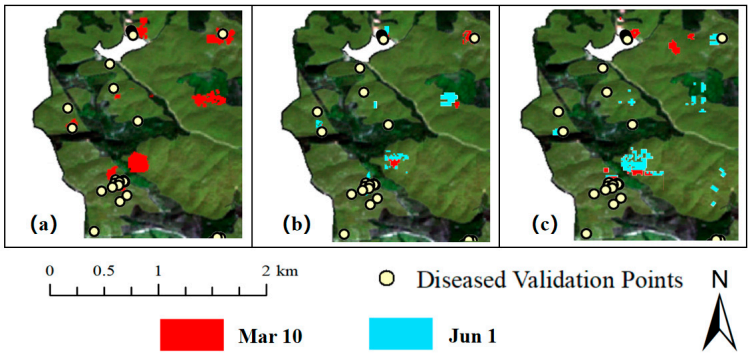

Figure 11. Temporal accuracy comparison of early infestation warning among three models: (**a**) At-T-LSTM, (**b**) EWMACD, and (**c**) COLD. Based on two consecutive remote sensing images (13 May 2019 and 7 June 2019), with red areas representing detection results from 13 May 2019 and blue areas from 7 June 2019.

4.4. Overall Detection Result

The overall detection results of anthracnose on *I. verum* in the study area are shown in Figure 12.

In Figure 12, the purple, pink, blue, yellow, orange, red, and brown patches represent the early monitoring results of *I. verum* anthracnose at 15-day intervals from the initial monitoring date, demonstrating the spatiotemporal diffusion dynamics of the disease. The anthracnose predominantly occurs on shaded slopes within the study area, likely due to insufficient solar radiation leading to weaker growth vigor of the trees and heightened disease susceptibility. Additionally, the disease exhibits contiguous infection patterns,

spreading radially from initial outbreak sites as epicenters—a pattern consistent with the intrinsic epidemiological characteristics of *I. verum* anthracnose.

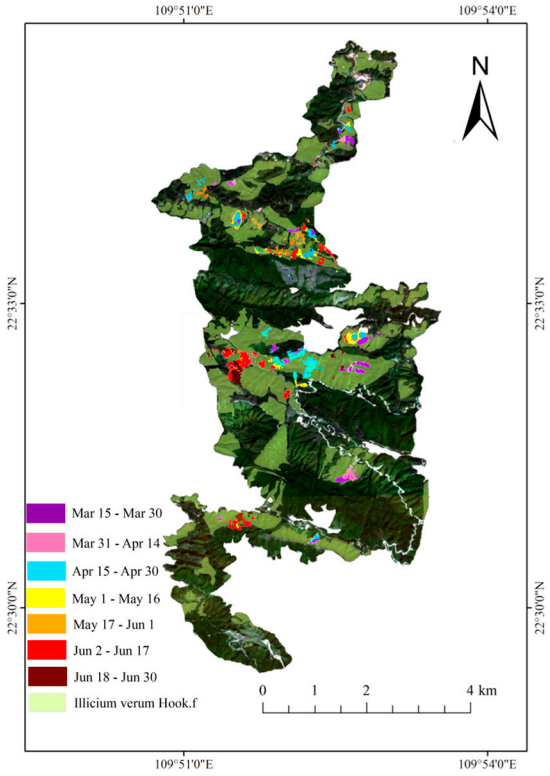

Figure 12. Overall early warning of infestation results in 2019.

5. Discussion

This study addresses the issue of sparse effective observations from optical remote sensing in cloud-prone and rainy regions, which compromises early warning systems for anthracnose on *I. verum*. By analyzing early-stage sensitive characteristics, we selected high-frequency environmental factors and anthracnose-sensitive remote sensing indicators as key features and introduced an Attention-based Time-Aware Long Short-Term Memory network to achieve early disease warnings. However, the approach still faces limitations.

Firstly, although Sentinel-2 optical imagery and high-frequency environmental data enhance temporal continuity for early warnings, persistent cloud cover causes extensive data gaps or prolonged observation intervals in cloud-prone and rainy regions, hindering the continuous monitoring of disease progression and anomaly detection. To improve spatiotemporal coverage, future research should incorporate Synthetic Aperture Radar (SAR) data. SAR enables all-weather imaging, penetrating clouds and rain to provide stable land surface information when optical data are unavailable. Moreover, existing studies demonstrate that SAR signals exhibit high sensitivity to vegetation structural changes, capturing potential indicators such as canopy structure alterations and moisture content variations induced by plant disease [48,49]. Therefore, integrating SAR data with environmental data is expected to significantly enhance the continuity of disease early warning models under complex climatic conditions.

Secondly, despite the effectiveness of the At-T-LSTM model in capturing temporal disease patterns through time-aware mechanisms and Self-Attention, its structural complexity and high parameter demand require large-scale, high-quality training data. With limited or noisy samples, the model risks overfitting and reduced generalization. Future studies could explore transfer learning [50,51]—pre-training on large generic time-series

datasets followed by fine-tuning on small anthracnose datasets—or data augmentation (e.g., via Conditional GANs) to reduce dependency on extensive labeled data and enhance robustness. Additionally, while Attention mechanisms enhance the model's ability to perceive critical temporal patterns, their "black-box" decision-making lacks interpretability, making it difficult to clarify the specific associations between meteorological factors or remote sensing features focused on at different time steps and disease progression, thereby limiting the model's verifiability and trustworthiness in practical early-warning systems.

Lastly, satellite-based monitoring operates at the stand-level due to spatial resolution constraints. Combining near-ground UAV imagery with deep learning could enable individual-tree-level detection, generating high-resolution infection maps for precision management [52,53]. Given UAVs' limited coverage, synergizing satellite and UAV data for large-scale early warning systems represents a critical future direction.

6. Conclusions

Timely monitoring and accurate delineation of spatial disease extent in early stages are essential for the effective management of *I. verum* anthracnose. This study demonstrates the value of integrating environmental variables (including meteorological and topographic factors) with Sentinel-2 time-series imagery through an Attention-based Temporal-Aware Long Short-Term Memory (At-T-LSTM) algorithm for early disease warning. The approach effectively captures subtle physiological changes in trees induced by anthracnose, even under challenging observational conditions.

The findings confirm that combining multisource features significantly enhances early detection capability. The model successfully handles irregular temporal intervals between environmental and remote sensing data, mitigating the constraint of sparse optical observations in cloudy regions. Experimental validation indicates a high level of reliability, with an F1-score of 0.86 for spatial delineation and 83% accuracy for temporal early-stage detection. These results underscore the potential of integrating ecological drivers with remote sensing time series for improving early warning systems in precision forestry. The framework offers a viable solution for monitoring forest diseases in persistently cloudy areas and supports the proactive management of *I. verum* anthracnose outbreaks.

Author Contributions: Conceptualization, J.L., Y.Z., L.W., and X.L.; methodology, Y.Z. and L.W.; software, J.L., T.Z., J.D., and Y.L.; validation, Y.Z., T.Z., and J.D.; format analysis, T.Z., J.D., and Y.L.; resources, J.L., L.W., and X.L.; data curation, Y.Z. and L.W.; writing—original draft preparation, J.L. and Y.Z.; writing—review and editing, L.W. and X.L.; supervision, X.L. All authors have read and agreed to the published version of the manuscript.

Funding: This research was founded by the Department of Forestry of Guangxi Zhuang Autonomous Region, grant number 2023GXZCLK20, and the Department of Science and Technology of Guangxi Zhuang Autonomous Region, grant number GXKJAA 24263014-2.

Data Availability Statement: The raw data supporting the conclusions of this article will be made available by the authors on request.

Acknowledgments: This work was supported by the High-performance Computing Platform of China University of Geoscience, Beijing. We thank the Google Earth Engine for providing Sentinel-2 data, the National Cryosphere Desert Data Center for providing the surface temperature and precipitation dataset, and ESRI for providing ESRI LULC products.

Conflicts of Interest: The authors declare no conflicts of interest.

References

1. Wang, G.W.; Hu, W.T.; Huang, B.K.; Qin, L.P. Illicium verum: A review on its botany, traditional use, chemistry and pharmacology. *J. Ethnopharmacol.* **2011**, *136*, 10–20. [CrossRef]
2. He, Z.; Huan, J.; Ye, M.; Liang, D.; Wu, Y.; Li, W.; Gong, X.; Jiang, L. Based on CiteSpace Insights into Illicium verum Hook. f. Current Hotspots and Emerging Trends and China Resources Distribution. *Foods* **2024**, *13*, 1510. [CrossRef]
3. Liao, W.; Luo, J.; Zou, D.; Zhong, Y.; Wu, Y.; Yan, K.; Huang, N. First Report of Anthracnose Caused by Colletotrichum siamense on Illicium verum in China. *Plant Dis.* **2023**, *107*, 2232. [CrossRef]
4. Li, J.; Zhong, Y.; Chen, J.; Ming, R.; Yao, S.; Li, L.; Tan, Y.; Huang, R.; Yao, C.; Huang, D. Genetic diversity analysis of Illicium verum germplasm resources in Guangxi based on SLAF-seq. *Guihaia* **2025**, *45*, 45730–45740. [CrossRef]
5. Lai, J.-L.; Bai, C.-H.; Pan, J.-M.; Du, F.-J.; Ning, S.; Xu, L.-Y.; Bei, Y.-J. Colletotrichum horii and Colletotrichum fioriniae Causing Anthracnose on Star Anise (Illicium verum) in China. *Plant Dis.* **2023**, *107*, 3294. [CrossRef]
6. Näsi, R.; Honkavaara, E.; Lyytikäinen-Saarenmaa, P.; Blomqvist, M.; Litkey, P.; Hakala, T.; Viljanen, N.; Kantola, T.; Tanhuanpää, T.; Holopainen, M. Using UAV-Based Photogrammetry and Hyperspectral Imaging for Mapping Bark Beetle Damage at Tree-Level. *Remote. Sens.* **2015**, *7*, 15467–15493. [CrossRef]
7. Mngadi, M.; Germishuizen, I.; Mutanga, O.; Naicker, R.; Maes, W.H.; Odebiri, O.; Schroder, M. A systematic review of the application of remote sensing technologies in mapping forest insect pests and diseases at a tree-level. *Sens. Appl. Soc. Environ.* **2024**, *36*, 101341. [CrossRef]
8. Sun, Z.; Ye, H.; Huang, W.; Qimuge, E.; Bai, H.; Nie, C.; Lu, L.; Qian, B.; Wu, B. Assessment on Potential Suitable Habitats of the Grasshopper Oedaleus decorus asiaticus in North China based on MaxEnt Modeling and Remote Sensing Data. *Insects* **2023**, *14*, 138. [CrossRef]
9. Luo, Y.; Huang, H.; Roques, A. Early Monitoring of Forest Wood-Boring Pests with Remote Sensing. *Annu. Rev. Èntomol.* **2023**, *68*, 277–298. [CrossRef]
10. Housman, I.W.; Chastain, R.A.; Finco, M.V. An evaluation of forest health insect and disease survey data and satellite-based remote sensing forest change detection methods: Case studies in the United States. *Remote. Sens.* **2018**, *10*, 1184. [CrossRef]
11. Thapa, B.; Wolter, P.T.; Sturtevant, B.R.; Townsend, P.A. Linking remote sensing and insect defoliation biology—A cross-system comparison. *Remote. Sens. Environ.* **2022**, *281*, 113236. [CrossRef]
12. Kovalev, A.; Tarasova, O.; Soukhovolsky, V.; Ivanova, Y. Is It Possible to Predict a Forest Insect Outbreak? Backtesting Using Remote Sensing Data. *Forests* **2024**, *15*, 1458. [CrossRef]
13. Lee, H.; Wintermantel, W.M.; Trumble, J.T.; Nansen, C. Timing matters: Remotely sensed vegetation greenness can predict insect vector migration and therefore outbreaks of curly top disease. *J. Pest Sci.* **2024**, *98*, 607–617. [CrossRef]
14. Marinelli, D.; Dalponte, M.; Frizzera, L.; Næsset, E.; Gianelle, D. A method for continuous sub-annual mapping of forest disturbances using optical time series. *Remote. Sens. Environ.* **2023**, *299*, 113852. [CrossRef]
15. Huo, L.N.; Persson, H.J.; Lindberg, E. Early detection of forest stress from European spruce bark beetle attack, and a new vegetation index: Normalized distance red & SWIR (NDRS). *Remote. Sens. Environ.* **2021**, *255*, 112240. [CrossRef]
16. Ye, S.; Rogan, J.; Zhu, Z.; Eastman, J.R. A near-real-time approach for monitoring forest disturbance using Landsat time series: Stochastic continuous change detection. *Remote. Sens. Environ.* **2021**, *252*, 112167. [CrossRef]
17. Li, M.; Liu, M.; Wang, X.; Liu, X.; Wu, L.; Li, J. Remote Sensing Recognition Model of Illicium verum Forest Pests and Diseases. *Sci. Silvae Sin.* **2024**, *60*, 128–138.
18. Zheng, Q.; Huang, W.; Xia, Q.; Dong, Y.; Ye, H.; Jiang, H.; Chen, S.; Huang, S. Remote Sensing Monitoring of Rice Diseases and Pests from Different Data Sources: A Review. *Agronomy* **2023**, *13*, 1851. [CrossRef]
19. Ren, C.; Liu, B.; Liang, Z.; Lin, Z.; Wang, W.; Wei, X.; Li, X.; Zou, X. An Innovative Method of Monitoring Cotton Aphid Infestation Based on Data Fusion and Multi-Source Remote Sensing Using Unmanned Aerial Vehicles. *Drones* **2025**, *9*, 229. [CrossRef]
20. Wang, D.; Sun, Z.; Huang, X.; Liu, M.; Zheng, Q.; Zhang, H.; Zhang, G. Pine wood nematode disease area identification based on multi-temporal multi-source remote sensing images and BIT model. *Geocarto Int.* **2024**, *39*, 2310117. [CrossRef]
21. Zhao, Y.; Cui, Z.; Liu, X.; Liu, M.; Yang, B.; Feng, L.; Zhou, B.; Zhang, T.; Tan, Z.; Wu, L. EWMACD Algorithm in Early Detection of Defoliation Caused by Dendrolimus tabulaeformis Tsai et Liu. *Remote. Sens.* **2024**, *16*, 2299. [CrossRef]
22. Shen, Y.Y.; Zhang, J.C.; Shen, D.; Tian, Y.Y.; Huang, W.J.; Yang, X.D. Research progress on habitat suitability assessment of crop diseases and pests by multi-source remote sensing information. *Chin. J. Eco-Agric.* **2023**, *31*, 1012–1025.
23. Wang, J.; Zhang, D. Intelligent pest forecasting with meteorological data: An explainable deep learning approach. *Expert Syst. Appl.* **2024**, *252*, 124137. [CrossRef]
24. Huang, S.; Liao, M.; Cen, Z.; Yan, W. Bionomics of aniseed anthracnose pathogen. *For. Pest Dis.* **2006**, *25*, 1–4. [CrossRef]
25. Liao, W.; Huang, N.; Zou, D.; Qin, S.; Jiang, X. Biological characteristics of pathogens of Colletotrichum horii for Illicium verum anthracnose. *For. Pest Dis.* **2018**, *37*, 10–12.
26. Lin, W.; Xu, M.F.; Quan, Y.B.; Liao, L.; Gao, L. Potential geographic distribution of Spodoptera frugiperda in China based on MaxEnt model. *Plant Quar.* **2019**, *33*, 69–73.

27. Meynard, C.N.; Gay, P.E.; Lecoq, M.; Foucart, A.; Piou, C.; Chapuis, M.P. Climate-driven geographic distribution of the desert locust during recession periods: Subspecies' niche differentiation and relative risks under scenarios of climate change. *Glob. Change Biol.* **2017**, *23*, 4739–4749. [CrossRef]
28. Shen, P.; Li, G. Risk assessment of *Bursaphelenchus xylophilus* in Hubei Province based on ecological niche factor analysis model. *J. Zhejiang AF Univ.* **2021**, *38*, 560–566.
29. Zhang, J.; Pu, R.; Yuan, L.; Huang, W.; Nie, C.; Yang, G. Integrating Remotely Sensed and Meteorological Observations to Forecast Wheat Powdery Mildew at a Regional Scale. *IEEE J. Sel. Top. Appl. Earth Obs.* **2014**, *7*, 4328–4339. [CrossRef]
30. Yuan, L.; Bao, Z.; Zhang, H.; Zhang, Y.; Liang, X. Habitat monitoring to evaluate crop disease and pest distributions based on multi-source satellite remote sensing imagery. *Optik* **2017**, *145*, 66–73. [CrossRef]
31. Silva, J.R.M.d.; Damásio, C.V.; Sousa, A.M.O.; Bugalho, L.; Pessanha, L.; Quaresma, P. Agriculture pest and disease risk maps considering MSG satellite data and land surface temperature. *Int. J. Appl. Earth Obs.* **2015**, *38*, 40–50. [CrossRef]
32. Bhattacharya, B.K.; Chattopadhyay, C. A multi-stage tracking for mustard rot disease combining surface meteorology and satellite remote sensing. *Comput. Electron. Agric.* **2013**, *90*, 35–44. [CrossRef]
33. Zhu, Z.; Zhang, J.; Yang, Z.; Aljaddani, A.H.; Cohen, W.B.; Qiu, S.; Zhou, C. Continuous monitoring of land disturbance based on Landsat time series. *Remote. Sens. Environ.* **2020**, *238*, 111116. [CrossRef]
34. Brooks, E.B.; Wynne, R.H.; Thomas, V.A. On-the-Fly Massively Multitemporal Change Detection Using Statistical Quality Control Charts and Landsat Data. *IEEE Trans. Geosci. Remote Sens.* **2014**, *52*, 3316–3332. [CrossRef]
35. Peng, D.; Liu, X.; Zhang, Y.; Guan, H.; Li, Y.; Bruzzone, L. Deep learning change detection techniques for optical remote sensing imagery: Status, perspectives and challenges. *Int. J. Appl. Earth Obs. Geoinf.* **2025**, *136*, 104282. [CrossRef]
36. Mou, L.; Zhao, P.; Xie, H.; Chen, Y. T-LSTM: A Long Short-Term Memory Neural Network Enhanced by Temporal Information for Traffic Flow Prediction. *IEEE Access* **2019**, *7*, 98053–98060. [CrossRef]
37. Saravana, L.; Ngo, Q.-H.; Zhang, J.; Vu, T.; Vu, T.L. Integrated attentive Bi-LSTM conditional GAN for power system oscillation localization. *Electr. Power Syst. Res.* **2025**, *242*, 111456. [CrossRef]
38. Qin, R.; Zhao, Z.; Xu, J.; Ye, J.-S.; Li, F.-M.; Zhang, F. HRLT: A high-resolution (1 day, 1 km) and long-term (1961–2019) gridded dataset for surface temperature and precipitation across China. *Earth Syst. Sci. Data* **2022**, *14*, 4793–4810. [CrossRef]
39. Wu, C.; Luo, L.; Li, W.; Li, W. Studies on Resistance of Different Cultivars of Rubber Tree against Colletotrichum gloeosporioides and Physiological Index after Its Control. *Acta Agric. Univ. Jiangxiensis* **2010**, *32*, 1152–1157.
40. Kuang, R.; Feng, H.; Sun, S.; Dan, Y.; Huang, Y.; Wang, J. Resistance of Camellia oleifera varieties to Colletotrichum gloeosporioides and its relations with physiological activities. *For. Pest Dis.* **2015**, *34*, 1–4. [CrossRef]
41. Chávez, R.; Rocco, R.; Gutiérrez, Á.; Dörner, M.; Estay, S. A Self-Calibrated Non-Parametric Time Series Analysis Approach for Assessing Insect Defoliation of Broad-Leaved Deciduous Nothofagus pumilio Forests. *Remote Sens.* **2019**, *11*, 204. [CrossRef]
42. Coops, N.C.; Johnson, M.; Wulder, M.A.; White, J.C. Assessment of QuickBird high spatial resolution imagery to detect red attack damage due to mountain pine beetle infestation. *Remote Sens. Environ.* **2006**, *103*, 67–80. [CrossRef]
43. Meigs, G.W.; Kennedy, R.E.; Cohen, W.B. A Landsat time series approach to characterize bark beetle and defoliator impacts on tree mortality and surface fuels in conifer forests. *Remote Sens. Environ.* **2011**, *115*, 3707–3718. [CrossRef]
44. Senf, C.; Pflugmacher, D.; Wulder, M.A.; Hostert, P. Characterizing spectral–temporal patterns of defoliator and bark beetle disturbances using Landsat time series. *Remote Sens. Environ.* **2015**, *170*, 166–177. [CrossRef]
45. Ma, X.; Huo, Z.; Lu, J.; Wong, Y.D. Deep Forest with SHapley additive explanations on detailed risky driving behavior data for freeway crash risk prediction. *Eng. Appl. Artif. Intell.* **2025**, *141*, 109787. [CrossRef]
46. Wang, Y.; Wang, Z.; Zhao, F. Integrating Node-Place Model With Shapley Additive Explanation for Metro Ridership Regression. *IEEE Trans. Intell. Transp. Syst.* **2025**, 1–10. [CrossRef]
47. Bathe, K.D.; Patil, N.S. ConvExNet: Deep learning-based flood detection utilizing Shapley additive explanations. *J. Earth Syst. Sci.* **2025**, *134*, 99. [CrossRef]
48. Tong, T.; Lin, S.; Li, L.; Luo, T.; Huang, H. Remote sensing recognition of pine wilt disease in Pinus massoniana forest combined with microwave and optical time series images. *J. Beijing For. Univ.* **2024**, *46*, 40–52.
49. Xue, J.; Yu, L.; Lin, Q.; Liu, G.; Huang, H. Using Sentinel-1 multi-temporal InSAR- data to monitor the damage degree of shoot beetle in Yunnan pine forest. *Remote Sens. Land Resour.* **2018**, *30*, 108–114.
50. Wang, H.; Chen, X.; Zhang, T.; Li, J.; Liu, K.; Wen, Z.; Kou, M.; Zhang, Y. CATNet: A Small Sample Transfer Learning Method for Key Point Detection of Blast Furnace Burden Surface. *ISIJ Int.* **2025**, *65*, 246–256. [CrossRef]
51. Liao, W.; Zhu, R.; Takiddin, A.; Tariq, M.; Ruan, G.; Cui, X.; Yang, Z. Transfer Learning-Driven Electricity Theft Detection in Small-Sample Cases. *IEEE Trans. Instrum. Meas.* **2024**, *73*, 2532013. [CrossRef]

52. Li, X.; Wang, A. Forest pest monitoring and early warning using UAV remote sensing and computer vision techniques. *Sci. Rep.* **2025**, *15*, 401. [CrossRef] [PubMed]
53. Zhu, H.; Zhu, H.; Lin, C.; Lin, C.; Liu, G.; Liu, G.; Wang, D.; Wang, D.; Qin, S.; Qin, S.; et al. Intelligent agriculture: Deep learning in UAV-based remote sensing imagery for crop diseases and pests detection. *Front. Plant Sci.* **2024**, *15*, 1435016. [CrossRef] [PubMed]

Disclaimer/Publisher's Note: The statements, opinions and data contained in all publications are solely those of the individual author(s) and contributor(s) and not of MDPI and/or the editor(s). MDPI and/or the editor(s) disclaim responsibility for any injury to people or property resulting from any ideas, methods, instructions or products referred to in the content.